

Enhanced tumor targeting effects of a novel paclitaxel-loaded polymer: PEG–PCCL-modified magnetic iron oxide nanoparticles

Xinyi Li^{a,b,*}, Yuan Yang^a, Yiping Jia^{a,c,*}, Xuan Pu^a, Ting Yang^a, Yicheng Wang^a, Xuefei Ma^a, Qi Chen^a, Mengwen Sun^a, Dapeng Wei^a, Yu Kuang^a, Yang Li^d and Yu Liu^d

^aDepartment of Microbiology, West China School of Basic Medical Sciences & Forensic Medicine, Sichuan University, Chengdu, China; ^bState Key Laboratory of Oral Diseases, National Clinical Research Center for Oral Diseases, Department of Orthodontics, West China Hospital of Stomatology, Sichuan University, Chengdu, China; ^cDepartment of Ultrasound, No.4 West China Teaching Hospital, Sichuan University, Chengdu, China; ^dSchool of Microelectronics and Solid-state Electronics, University of Electronic Science and Technology of China, Chengdu, China

ABSTRACT

Background: Multifunctional magnetic nanoparticles (MNP) have been newly developed for tumor-targeted drug carriers. To address challenges including biocompatibility, stability, nontoxicity, and targeting efficiency, here we report the novel drug deliverer poly(ethylene glycol) carboxyl–poly(ϵ -caprolactone) modified MNP (PEG–PCCL–MNP) suitable for magnetic targeting based on our previous studies.

Methods: Their *in vitro* characterization and cytotoxicity assessments, *in vivo* cytotoxicity assessments, and antitumor efficacy study were elaborately investigated.

Results: The size of PEG–PCCL–MNP was 79.6 ± 0.945 nm. PEG–PCCL–MNP showed little *in vitro* or *in vivo* cytotoxicity and good biocompatibility, as well as effective tumor-specific cell targeting for drug delivery with the presence of external magnetic field.

Discussion: PEG–PCCL–MNP is a potential candidate of biocompatible and tumor-specific targeting drug vehicle for hydrophobic drugs.

ARTICLE HISTORY

Received 3 August 2017
Revised 20 August 2017
Accepted 25 August 2017

KEYWORDS

Magnetic nanoparticle; carrier; cytotoxicity; biocompatibility; tumor-target

1. Introduction

Magnetic nanoparticles (MNPs) have been investigated for ‘theranostics’, which means combining both diagnostic and therapeutic capabilities into a single agent (Del Vecchio et al., 2007). The superior magnetic properties of MNPs, along with their inherent biocompatibility and inexpensiveness, have made MNPs a material of choice in many biomedical applications (Xie et al., 2010), such as contrast probes for magnetic resonance imaging (MRI) and tumor-specific cell targeting for drug delivery (Cole et al., 2011). Despite significant advances made in the use of MNP over the past 10 years, challenges still remain in fabricating and processing magnetic iron oxide nanoparticles that are suitable for *in vivo* medical applications. Notably, the issues of biocompatibility, stability, nontoxicity, and targeting efficiency must be addressed (Sun et al., 2010). These challenges become more outstanding as MNPs possess a high surface area-to-volume ratio, which offers high loading capacity of functional cargoes including drugs (Cole et al., 2011), but in turn leads to aggregate and absorb plasma proteins upon intravenous injection, resulting in rapid clearance by the reticuloendothelial system (Moore et al., 2000). Thus, these MNPs are commonly coated with a polymer to improve their dispersity and stability.

PEG was supposed to be promising coating materials for such purposes used in drug delivery systems because of the ability to offer a steric barrier to protein adsorption, leading to reduced uptake by macrophages of the reticuloendothelial system and ultimately, increased serum half-life (Larsen et al., 2009). Additionally, some diblock and triblock polymers have also been investigated such as monomethoxy poly(ethylene glycol)–poly(ϵ -caprolactone) (MPEG–PCL) (Qiu et al., 2013), PEG–PCL–PEG (Luo et al., 2016), and PCL–PEG–PCL (Wang et al., 2012). While encapsulated with the hydrophobic drug like paclitaxel, the hydrophobic PCL combined with the drug forms the core of nanoparticles and the hydrophilic PEG forms the shell, thus making the drug intravenously injectable (Gou et al., 2011).

We have previously prepared hyper-branched polyethyleneimine-graftpolycaprolactone-block-mono-methoxyl-poly(ethylene glycol) copolymers (hy-PEI-PCL-mPEG) and PEG–MNP (Liu et al., 2011; Kuang et al., 2012). Based on our present study, unlike the above-mentioned coating materials, PEG–PCCL which is additionally carboxyl covalently modified on the caprolactone tends to be more hydrophilic and more stable due to effect of the hydrogen bond. Meanwhile, because the toxicity assay of nanoparticles is necessary in a set of design rules for predictive models and validated standard methods,

CONTACT Yu Liu  poly1634@hotmail.com  School of Microelectronics and Solid-state Electronics, University of Electronic Science and Technology of China, Chengdu, China; Yuan Yang  yangyuan1114@163.com  Department of Microbiology, West China School of Basic Medical Sciences & Forensic Medicine, Sichuan University, Chengdu, China

*These authors contributed equally to this work.

© 2017 The Author(s). Published by Informa UK Limited, trading as Taylor & Francis Group.

This is an Open Access article distributed under the terms of the Creative Commons Attribution-NonCommercial License (<http://creativecommons.org/licenses/by-nc/4.0/>), which permits unrestricted non-commercial use, distribution, and reproduction in any medium, provided the original work is properly cited.

we demonstrated that PEG-PCCL nanospheres showed less cytotoxicity and better biocompatibility than mature medical nanoparticles (PEI) at the therapeutical concentration and PEG-PCCL-loaded PTX revealed good treatment effect on tumor growth by inducing apoptosis, which suggested that PEG-PCCL is a potential candidate of biocompatible drug vehicle for hydrophobic drugs.

Therefore, in the present work, we focused on how to improve the target property of PEG-PCCL and remove the application barriers of MNPs *in vivo*. So we embedded the PEG-PCCL polymers on the surface of ferriferrous oxide to form a core shell structure and systemic toxicity assessments were performed qualitatively and quantitatively to show the biocompatibility and acute biotoxicity. We have focused on systemic toxicity assessments of PEG-PCCL in another study and some parts of the results was provided as negative control in the present research. The static magnetic field has also been used to show the increase in accumulation in murine tumors when compared with the conventional target system. Additionally, because paclitaxel (PTX) is a first-line anti-cancer drug especially ovarian cancer and non-small cell lung cancer, and has been listed in the World Health Organization's List of Essential Medicines (Zhang et al., 2016), so PTX-loaded PEG-PCCL-MNP was used to examine the antitumor effect *in vivo* in hepatic H22 tumor-bearing mice model.

2. Materials and methods

2.1. Materials and animals

ϵ -Caprolactone (ϵ -CL, Alfa Aesar, Ward Hill, MA), poly(ethylene glycol) (PEG, MW 6000, Fluka, St. Louis, MO), Dulbecco's modified Eagle's medium (DMEM, Hyclone, South Logan, UT), 3-(4,5-dimethylthiazol-2-yl)-2,5-diphenyl tetrazolium bromide (MTT, Sigma, St. Louis, MO), fetal bovine serum (FBS, Hyclone, UT) were used without further purification. Mouse H22 hepatocarcinoma cells (H22), human embryonic kidney cells (HEK293T), and hepatoma carcinoma cell (Hep G2) were obtained from Department of Immunology, West China

School of Preclinical and Forensic Medicine, Sichuan University. All the materials were of analytic reagent grade.

Male BALB/c mice (4–6 weeks old, 20–25 g weight) and New Zealand rabbit (2.5–3.0 kg weight) were purchased from the Chengdu DaShuo biotech companies (SiChuan, Chengdu, Sichuan, China) with Certificate of Quality No. SCXK2013-24. All animal experiments complied with the Animal Management Rules of the Ministry of Health of the People's Republic of China. All of the animal experimental procedures were approved by the Ethical Committee for Laboratory Animals of West China medical center of Sichuan University.

2.2. Preparation and characterization of PEG-PCCL-MNP

PEG-PCCL-MNP and PEG-PCCL were supplied by our cooperator, Professor Liu from School of Microelectronics and Solid-state Electronics, University of Electronic Science and Technology of China. The process for preparing PEG-PCCL-MNP nanoparticles by controlled chemical coprecipitation is schematically illustrated in Figure 1.

First, amphiphilic cationic copolymer PEG-PCL-g-Imi was synthesized which included two blocks, PEG and PCL-g-Imi. The side chains of the PCL-g-Imi block had hydroxyl group and imidazole group (Imi). Similarly, amphiphilic anionic copolymer PEG-PCCL was synthesized which also included two blocks PEG and PCCL. The side chains of the PCCL block had carboxyl group. Then, Fe^{2+} , Fe^{3+} , and PEG-PCL-g-Imi were used to obtain magnetic nanoparticles which surface charge is positive by improved coprecipitation method. Finally, anionic polymer PEG-PCCL was added and PEG-PCCL-MNP was acquired by self assembly. The PTX-loaded PEG-PCCL-MNP nanoparticles were prepared by the solvent diffusion method.

The particle size, polydispersity index (PDI) and zeta potential of PEG-PCCL-MNP and PEG-PCCL were measured with laser particle size analyzer (Malvern Nano-ZS 90). Transmission electron microscopy (TEM, H-6009IV, Hitachi, Japan) was used to assess the morphology of the PEG-PCCL-MNP and PEG-PCCL. The PTX entrapment efficiency (EE) was measured with minicolumn centrifugation

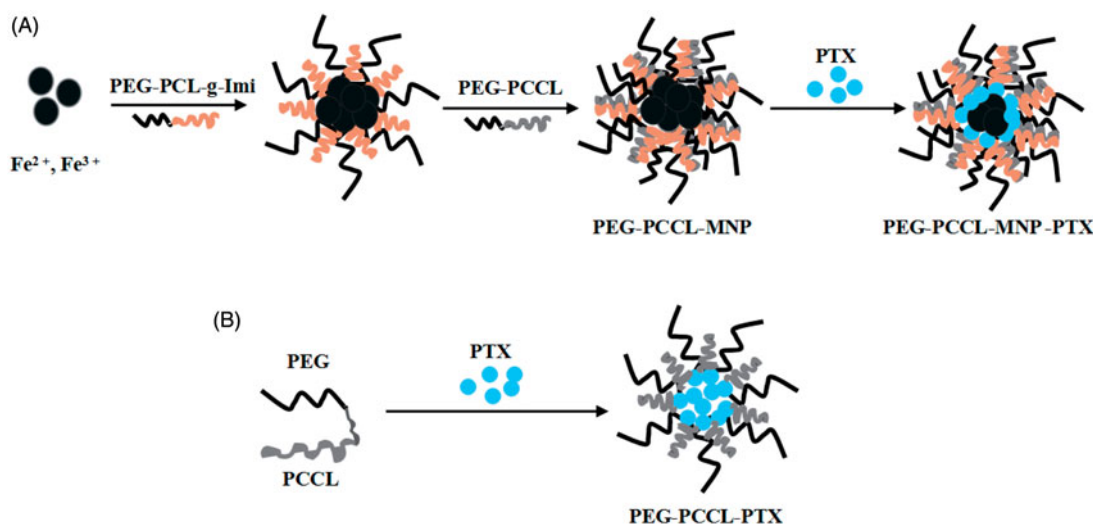


Figure 1. Synthesis schematic of PEG-PCCL-MNP, PEG-PCCL, and their PTX-loaded nanoparticles. (A) PEG-PCCL-MNP (B) PEG-PCCL.

method (Li et al., 2008). The concentrations of PTX incorporated in PEG-PCCL-MNP/PEG-PCCL (C) and the total drug in PEG-PCCL-MNP/PEG-PCCL dispersions (C_0) were analyzed by HPLC, respectively. EE was calculated by the following equation:

$$EE (\%) = \frac{C}{C_0} \times 100\%$$

2.3. In vitro cytotoxicity assessments

2.3.1. Cellular uptake studies

HepG2 and HEK293 cells were seeded in 12-well plates at a density of 1×10^4 cells per well respectively and incubated at 37 °C for 24 h to allow attachment. Then the cells were washed with PBS twice and incubated with PEG-PCCL-MNP (0.5 mg/ml) at 37 °C for 24 h (Danhier et al., 2009). At the end of incubation, the cells were obtained by trypsinization and then samples were centrifuged, fixed, and stained with lead citrate and uranium acetate and then photographed by TEM.

2.3.2. MTT assays

The cytotoxicity of PEG-PCCL-MNP was determined through the HepG2 and HEK293 cells viability using MTT assays (Xu et al., 2010). The cells were cultivated in 96-well plates at a density of 10^4 cells per well in DMEM medium overnight. Then the medium was replaced by PEG-PCCL and PEG-PCCL-MNP, respectively of different concentrations ranging from 0.25 to 1 mg/ml dissolved in serum-free medium. After incubation for 4 h, the plates were washed with PBS and replaced by serum-free medium. Following cultivation in incubator overnight, MTT assay was performed according to the instruction. The absorbance values were measured with the spectrophotometer reader at 570 nm. All experiments were performed in triplicate. Cell viability was expressed as:

$$\text{Cell viability (\%)} = \frac{OD_T}{OD_C} \times 100\%$$

where OD_T stands for the absorbance intensity of cells treated with PEG-PCCL and PEG-PCCL-MNP copolymers, and OD_C stands for the absorbance intensity of cells incubated only with the medium.

2.3.3. Annexin V/PI apoptosis cell death assays

Apoptosis was determined by Annexin V-FITC and PI double staining (van Heerde et al., 1995). Briefly, HEK293 cells were seeded in 12-well plates at a density of 1×10^4 cells/well and treated with PEG-PCCL (0.5 mg/ml) and PEG-PCCL-MNP (0.5 mg/ml) for 4 h. Then the cells were washed with PBS for three times, followed by Annexin V-FITC incubation for 15 min and PI staining for another 15 min at 4 °C in the dark. The stained cells were observed under fluorescence microscope (Olympus Co. Ltd., Tokyo, Japan) within 30 min.

2.3.4. Hemolysis assays

The haemocompatibility of PEG-PCCL-MNP was evaluated according to the *in vitro* red blood cell (RBC) hemolysis test.

The blood sample were collected from the rabbit and white cells were removed. Finally erythrocytes were dissolved in PBS at 2% concentration and mixed with an equal volume physiologic saline, PEG-PCCL, and PEG-PCCL-MNP of 0.5 mg/ml, respectively. A positive hemolysis control was prepared by adding an equal volume of erythrocyte suspension and distilled water. After the mixture was maintained for 1 and 3 h at 37 °C and then centrifuged at 2000 r/min for 5 min, the supernatants were detected with a microplate reader (Bio-Rad, Hercules, CA) at 570 nm. The percentage of hemolysis was calculated by the equation:

$$\text{Hemolysis (\%)} = \frac{OD_T - OD_{NC}}{OD_{PC} - OD_{NC}} \times 100\%$$

where OD_T , OD_{NC} , OD_{PC} refer to the absorbance values of sample, negative control, and positive control, respectively.

2.4. In vivo cytotoxicity assessments

2.4.1. Rabbit phlebitis

The rabbits were divided into three groups randomly and given 1 ml physiologic saline, 0.5 mg/ml PEG-PCCL, and 0.5 mg/ml PEG-PCCL-MNP, respectively *via* auricular vein. Then the tissues which was 2 cm anterior to the injection site were obtained after 24 h and then fixed with 4% paraformaldehyde for HE staining. Histopathological examination was performed blindly to evaluate the inflammation and vein through the observation under light microscope.

2.4.2. Histological examination of organs

Twenty-four BALB/c mice were divided into three groups randomly. PEG-PCCL-MNP suspension (20 mg/kg), PEG-PCCL suspension (20 mg/kg), and an equal volume of physiologic saline were given to mice group, respectively *via* tail vein. The group which was given the PEG-PCCL-MNP was attached with a neodymium-iron-boron (NdFeB) permanent magnet to provide an external static magnetic field (1.7T) fixed to the surface of the extrahepatic skin. After 1, 3, 6, 12, 24, 48 h, mice were sacrificed by cervical dislocation to evaluate acute inflammation and biodistribution. The samples of liver, lung, spleen, and kidney were obtained and preserved with 4% paraformaldehyde and then embedded in paraffin for HE staining and Prussian blue staining. The histopathological changes were observed under light microscope and recorded with assorted camera (Leica, Co. Ltd., Wetzlar, Germany).

2.5. In vivo antitumor efficacy study

Antitumor efficacy of PEG-PCCL-MNP/PTX was investigated in BALB/c mice (Wang et al., 2013), which were developed by injection of H22 cells suspension (0.25 ml, 4×10^6 cells/mouse) subcutaneously in the left armpits of BALB/c mice. When the tumor size reached a volume of approximately 0.30 cm³, transplanted mice were randomly divided into four groups ($n=5$) for different treatment. They were injected with normal saline, PTX (10 mg/kg), PEG-PCCL/PTX (20 mg/kg), and PEG-PCCL-MNP/PTX (20 mg/kg) once every two days *via* tail vein at a dose of 0.5 ml. Meanwhile, the

Table 1A. Characterization of PEG-PCCL-MNP (mean \pm SD, $n = 3$).

Samples	Particle size (nm)	PDI	Zeta potential (mV)	Conductivity (mS/cm)	EE (%)
PEG-PCCL	79.60 \pm 0.95	0.336	-18.40 \pm 6.32	0.0142	55.98
PEG-PCCL-MNP	86.39 \pm 0.94	0.370	-23.50 \pm 5.44	0.0196	59.72

Table 1B. The renal function of PEG-PCCL-MNP (mean \pm SD, $n = 3$).

Samples	Carbamide (mmol/L)	Creatinine (μ mol/L)	Lithic acid (μ mol/L)
NS	3.91 \pm 0.41	5.53 \pm 0.35	16.53 \pm 3.64
PEG-PCCL	1.64 \pm 0.23	2.02 \pm 0.18	13.15 \pm 4.31
PEG-PCCL-MNP	2.07 \pm 0.26	5.57 \pm 0.26	15.87 \pm 3.27

PEG-PCCL-MNP/PTX group was given a static magnetic field (1.7T) which was produced by a neodymium-iron-boron (NdFeB) permanent magnet fixed to the surface of the left armpits skin.

2.5.1. Tumor inhibition evaluation

Tumor volume of each mouse was measured with a digital caliper daily during the process and was calculated by the formula:

$$V_{\text{tumor}} = \frac{A^2 \times B}{2}$$

where A and B denote the shortest and longest diameter (mm) of the tumor, respectively. Tumor volume-time curve was obtained from days 0 to 11 after administration.

All the mice were sacrificed by cervical dislocation on day 11 and the tumors were removed, washed by saline, and recorded on the weight. We also checked whether there is metastasis in peripheral lymph nodes and major organs. Inhibition rate was calculated by the formula:

$$\text{Inhibition rate (\%)} = \frac{W_C - W_T}{W_C} \times 100\%$$

where W_C is the tumor weight of control group and W_T is the tumor weight of treatment group.

2.5.2. Histological detection of apoptosis

The tissues of liver, lung, spleen, kidney, and inguinal glands were fixed and embedded immediately. The samples were processed for apoptosis of DNA by the (TdT-mediated dUTP nick end labeling) TUNEL method using Tunel-POD kits according to the manufacturer's instructions. The nuclei of cells with apoptosis are positively stained with yellow color and the negative ones with blue color.

2.5.3. Safety studies

To evaluate the toxicity of PEG-PCCL-MNP/PTX treatment, as indicated by loss of body weight, each mouse was weighed every day and body weight versus time curve was established.

2.6. Statistical analysis

Statistical analysis was performed with SPSS 19.0. (IBM, New York, NY). Every experimental treatment was repeated

independently for at least three times. All results were expressed as mean \pm SD. Both independent sample t -test and One-Way ANOVA were utilized for statistical analysis. Statistical significance was indicated at $p < .05$.

3. Results

3.1. Characterization of PEG-PCCL-MNP

Table 1A summarizes the mean diameter, PDI, zeta potential of PEG-PCCL, PEG-PCCL-MNP, and EE of PTX-loaded nanoparticles.

As shown in microphotographs of nanoparticles using transmission electron microscope, PEG-PCCL and PEG-PCCL-MNP had morphology of a round and homogeneous shape under TEM.

3.2. In vitro cytotoxicity assessments

Most nanoparticles have characterizations of instability and tendency of aggregation which may change the way in which they pass through the cell membranes (Elsaesser & Howard, 2012). Thus, the investigation of the uptake of PEG-PCCL-MNP by HepG2 and HEK293 cells was performed and observed under TEM, as shown in Figure 2.

To investigate the effect of PEG-PCCL-MNP and PEG-PCCL on the viability of cells, MTT assay was performed and depicted in Figure 3(A,B).

Cells could be damaged by nanoparticles both chemically and physically. And apoptosis is correlated with changes in morphology and biochemistry, including cell shrinkage, cell surface changes, DNA fragmentation, and chromatin condensation (Gregory & Pound, 2010). In the apoptosis assays, as Figure 3(C) shows, though compared with the blank control group, the polymers groups induced early apoptosis, no obvious necrosis could be seen in both the PEG-PCCL and PEG-PCCL-MNP groups. Importantly, there was no significant difference in ability to induce early apoptosis between PEG-PCCL and PEG-PCCL-MNP by cell counting ($p > .05$), which was consistent with the results of previously conducted MTT assay.

In vitro hemolysis assay is a necessary part of early preclinical research, as hemolysis can lead to jaundice, anemia, and other abnormal conditions (Dobrovolskaia et al., 2008). As shown in Figure 3(D), no significant hemolysis of erythrocytes over 3 h incubation was observed by neither PEG-PCCL nor PEG-PCCL-MNP at the concentration of 0.5 mg/ml when compared with the normal saline group. PEG-PCCL-MNP only caused slight hemolysis (3%) at 1 h and after that,

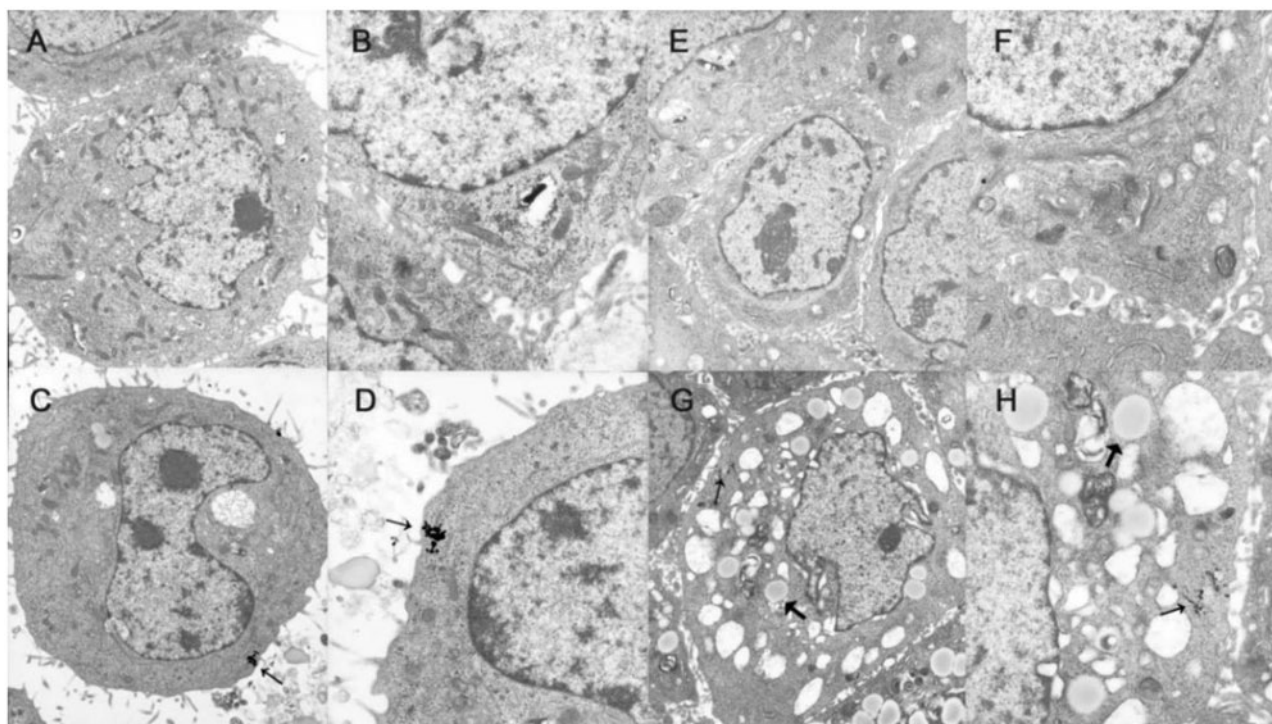


Figure 2. Uptake image of PEG-PCCL-MNP by cells using transmission electron microscope. (A/B): normal HepG2 cells; (C/D): HepG2 cells treated with PEG-PCCL-MNP polymers; (E/F): normal HEK293 cells; (G/H): HEK293 cells treated with PEG-PCCL-MNP polymers (black arrow represents iron oxide particles; thick black arrow represents endosome of nanoparticles. Image A/C/E/G 6000 \times , Image B/D/F/H 12,000 \times).

interestingly, no more hemolysis could be observed. Furthermore, as time went by, hemolysis of PEG-PCCL and physiological saline increased while that of PEG-PCL-MNP decreased.

3.3. In vivo cytotoxicity assessments

The degree of acute and excessive inflammation can reveal biocompatibility and toxicity of nanoparticles. As shown in Figure 4(a) of rabbit phlebitis studies, compared with the blank control, the PEG-PCCL-MNP and PEG-PCCL did not induce acute inflammatory infiltration near veins, edema, or loss of venous endothelial cells. Meanwhile, both the PEG-PCCL and PEG-PCCL-MNP did not induce significant cartilage degeneration.

Figure 4(b) illustrates the morphology of lung, liver, spleen, and kidney after injection with nanoparticles. In pulmonary tissue, no obvious cellular immunogenic response, pulmonary interstitial hyperplasia, or exudation in alveolar cavity was observed in both the PEG-PCCL and PEG-PCCL-MNP groups, compared with the blank control group. Similarly, in liver tissues, PEG-PCCL and PEG-PCCL-MNP did not induce significant hydropic degeneration or fatty change. However, in spleen, it was strange that there should have been more nanoparticles due to the particle size and reticuloendothelial system scavenging, which will be discussed in the followed part. Moreover, little acute proliferation, basement membrane thickening, inflammatory exudation, hyalinosis, or sclerosis can be seen in kidney, however, when we further check the renal function, PEG-PCCL and PEG-PCCL-MNP have little toxicity compared with physiological saline group (Table 1B).

Through Prussian blue staining, PEG-PCCL-MNP is stained blue for evaluation of biodistribution. PEG-PCCL-MNP has higher distribution in liver at 12 h than other tissues after injection of nanoparticles intravenous at the site of tail vein (Figure 4(c)).

3.4. In vivo antitumor efficacy study

The tumor growing curves of different groups were acquired as shown in Figure 5(A). The tumor growing rates of mice increased in the following sequence: PEG-PCCL-MNP/PTX < PEG-PCCL/PTX < PTX < saline.

The average tumor weight at the end of treatment was 1.98 ± 0.11 , 1.61 ± 0.13 , 1.40 ± 0.06 , 1.28 ± 0.10 g for saline, PTX, PEG-PCCL/PTX, PEG-PCCL-MNP/PTX, respectively (Figure 5(B)). In contrast to the saline group, the PTX, PEG-PCCL/PTX, and PEG-PCCL-MNP/PTX groups exhibited remarkable difference in tumor weight ($p < .05$, $p < .001$, $p < .001$). And inhibition rates of the PTX, PEG-PCCL/PTX, and PEG-PCCL-MNP/PTX groups were 7.12%, 30.78%, and 45.23%, respectively.

The changes in body weight over time for all groups are summarized in Figure 5(C).

Metastasis of tumors was not observed significantly in all the groups, which was related to the time setting of the end of the experiment.

Besides, drug-loaded nanoparticles showed an enhancement on apoptosis of tumor cells ($p < .05$) compared with the mere PTX group. Furthermore, the PEG-PCCL-MNP/PTX nanospheres group, with the presence of external static magnetic field, showed a significant increased induction on the apoptosis of tumors than the PEG-PCCL/PTX group. Coagulative areas of apoptosis were observed significantly among the PTX, PEG-PCCL/PTX, and PEG-PCCL-MNP/PTX

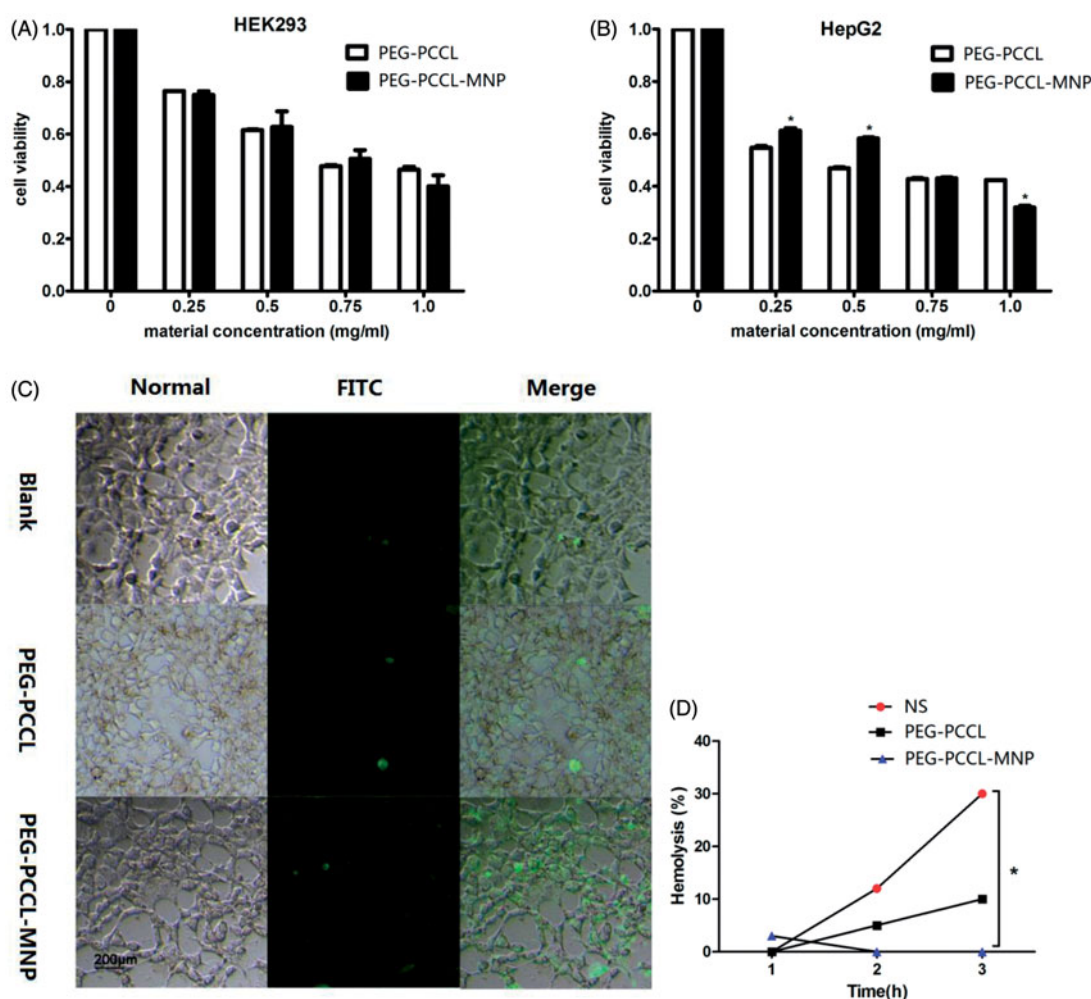


Figure 3. Effect on the cell viability of the nanoparticles on different cells by MTT assays. (A) HEK 293 cells treated with PEG-PCCL and PEG-PCCL-MNP; (B) HepG2 cells treated with PEG-PCCL and PEG-PCCL-MNP. (C) Annexin V/PI apoptosis detection after PEG-PCCL (0.5 mg/ml) and PEG-PCCL-MNP (0.5 mg/ml) treatment for 4 h. Cells stained green represents early apoptosis and cells stained red represents necrosis. (D) Hemolysis ratio *in vitro* after PEG-PCCL (0.5 mg/ml) and PEG-PCCL-MNP (0.5 mg/ml) treatment by different time.

groups, compared with the saline groups, which indicated that treatments with drugs were effective. As can be seen in Figure 4(d), not only massive apoptosis but also some bubbles-like structures could be observed in tumors tissues from the PEG-PCCL-MNP/PTX group, which will be discussed.

4. Discussions

Several merits of magnetic materials modified by biodegradable polymers, such as PEG, make them attractive candidates for delivering anti-cancer drugs to tumors, primarily owing to their comparable biocompatibility, dispersion, colloidal stability, and targeted delivery. This research is the first to put forward the idea coating MNPs with PEG-PCCL to decrease toxicity and improve dispersity and stability of MNPs. In the current report, PTX was chosen as the loaded drug and novel PEG-PCCL in our previous study was successfully prepared. The physicochemical properties, *in vitro* cytotoxicity assessments, *in vivo* cytotoxicity assessments, and *in vivo* antitumor efficacy study of PEG-PCCL-MNP were amply assessed.

The average size of PEG-PCCL-MNP was 79 nm, smaller than PEG-PCCL (86 nm). This may be because the MNP enlarged the size of the particles. Particle size is a key influence factor

of the carriers (Rahman et al., 2013). It has impacts on the *in vitro* and *in vivo* efficiency of the nanoparticles, including decreased uptake by the liver, prolonged blood circulation time, and improved bioavailability. The average size results of these two polymers indicated that they were blood vessels permeable. The test was repeated with the same solution two weeks later, and similar size distributions were detected, which suggested that conditions of PEG-PCCL and PEG-PCCL-MNP were relatively stable in the solution (Liu et al., 2014). The PDI values, as an important measure of the width of molecular weight distributions (MWD) (Rogošić et al., 1996), of both our nanoparticles were relatively low, indicating that they had a relatively mean nanoparticle size. The zeta potential of PEG-PCCL-MNP was less than that of PEG-PCCL, representing that PEG-PCCL-MNP had a higher nanoparticle stability from aggregation (Liu et al., 2014). The EE_{PTX} in both PEG-PCCL-MNP/PTX and PEG-PCCL/PTX was over 50%. This could be the evidence that the conjugation of MNP did not have a passive effect on the encapsulation of PTX. The high EE achieved could offer advantages in the drug delivery *in vitro* and *in vivo*. As for morphology, PEG-PCCL and PEG-PCCL-MNP had a round and homogeneous shape under TEM. Though some nanoparticles failed

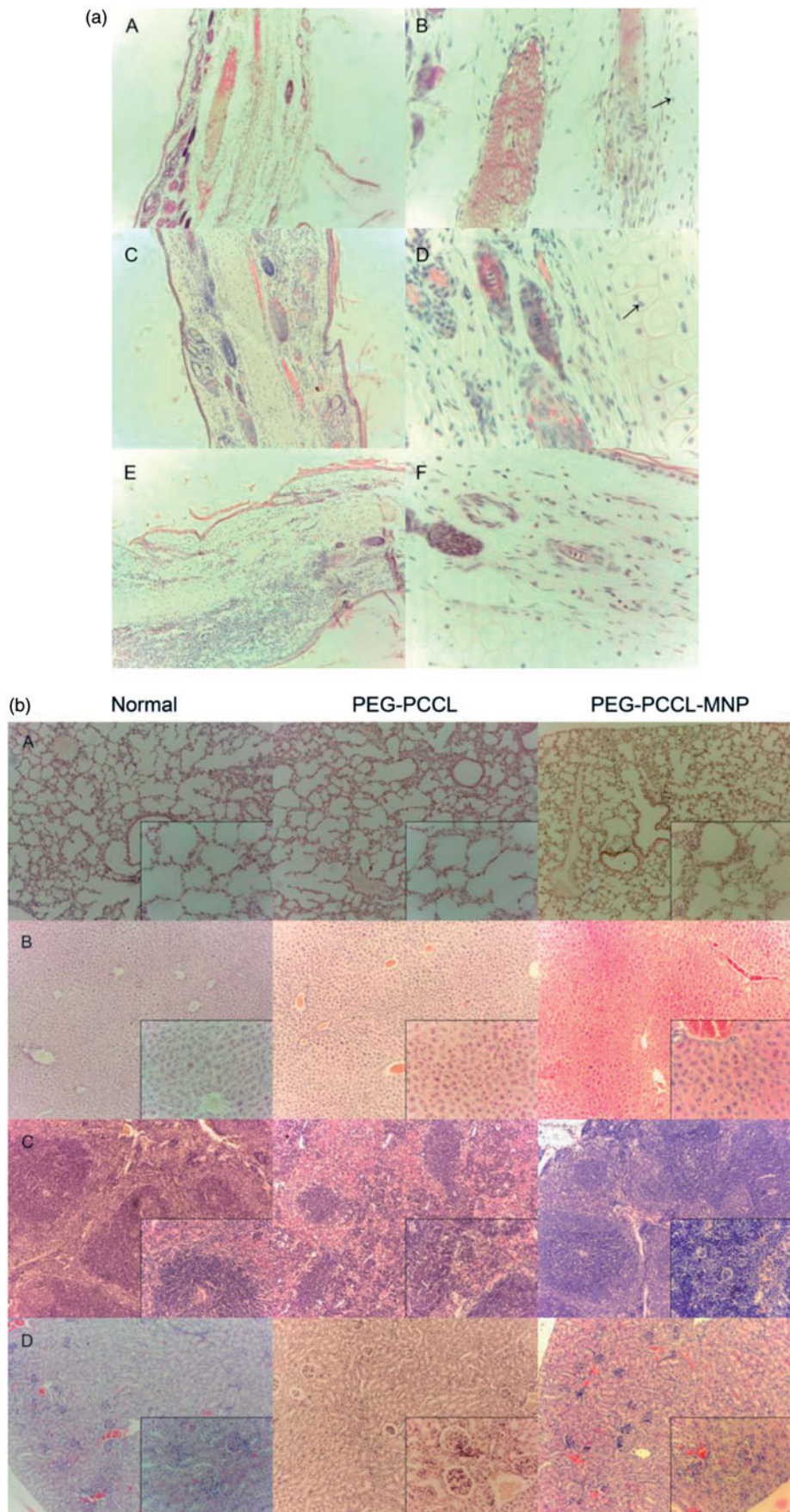


Figure 4. (a) Photomicrographs of the ear vein after 24 h treatment with polymers stained by H&E. (A/B) normal saline (C/D) PEG-PCCL (E/F) PEG-PCCL-MNP (black arrows point at cartilage, left image 10 \times , right image 40 \times). (b) The H&E staining images of different tissue under light microscope. (A) Lung, (B) liver, (C) spleen, (D) kidney (larger image 10 \times , inset box 40 \times). (c) Prussian blue staining of different tissue (iron oxide particles are stained blue). (A/B) Lung, (C/D) liver, (E/F) spleen, (G/H) kidney (left image 10 \times , right image 40 \times). (d) Light microscopy examination tumor slices of different treatment after TUNEL staining. (A) Normal saline, (B) PTX, (C) PEG-PCCL/PTX, (D) PEG-PCCL-MNP/PTX (black arrow points out necrosis of tumor cells. Larger image 10 \times , inset box 40 \times).

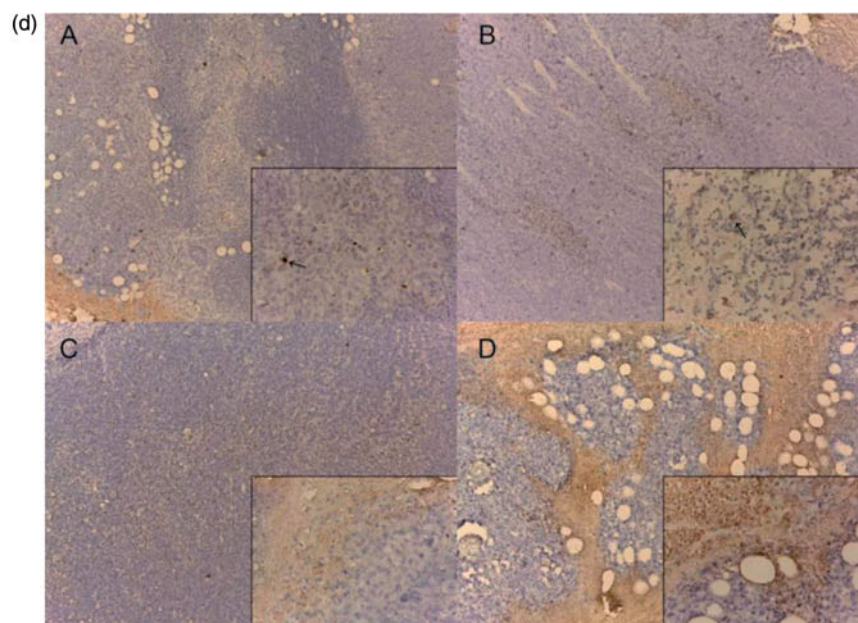
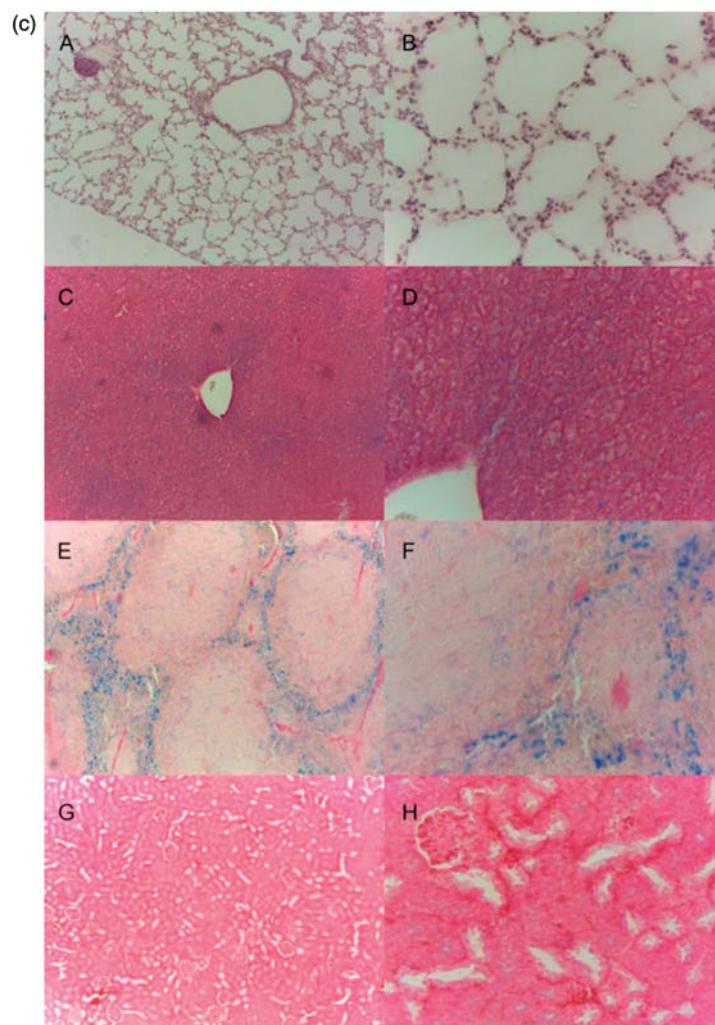


Figure 4. Continued.

to encapsulate iron oxide particles, there were successfully obtained PEG-PCCL-MNP polymers.

In *in vitro* cytotoxicity assessments, the cellular uptake study (Figure 2) demonstrated the presence of iron oxide

particles in the intracellular compartment in both HepG2 and HEK293, recognized by dark spots under TEM, which indicated that our nanoparticles were able to enter into cells by endocytosis (Elsaesser & Howard, 2012). Furthermore, the

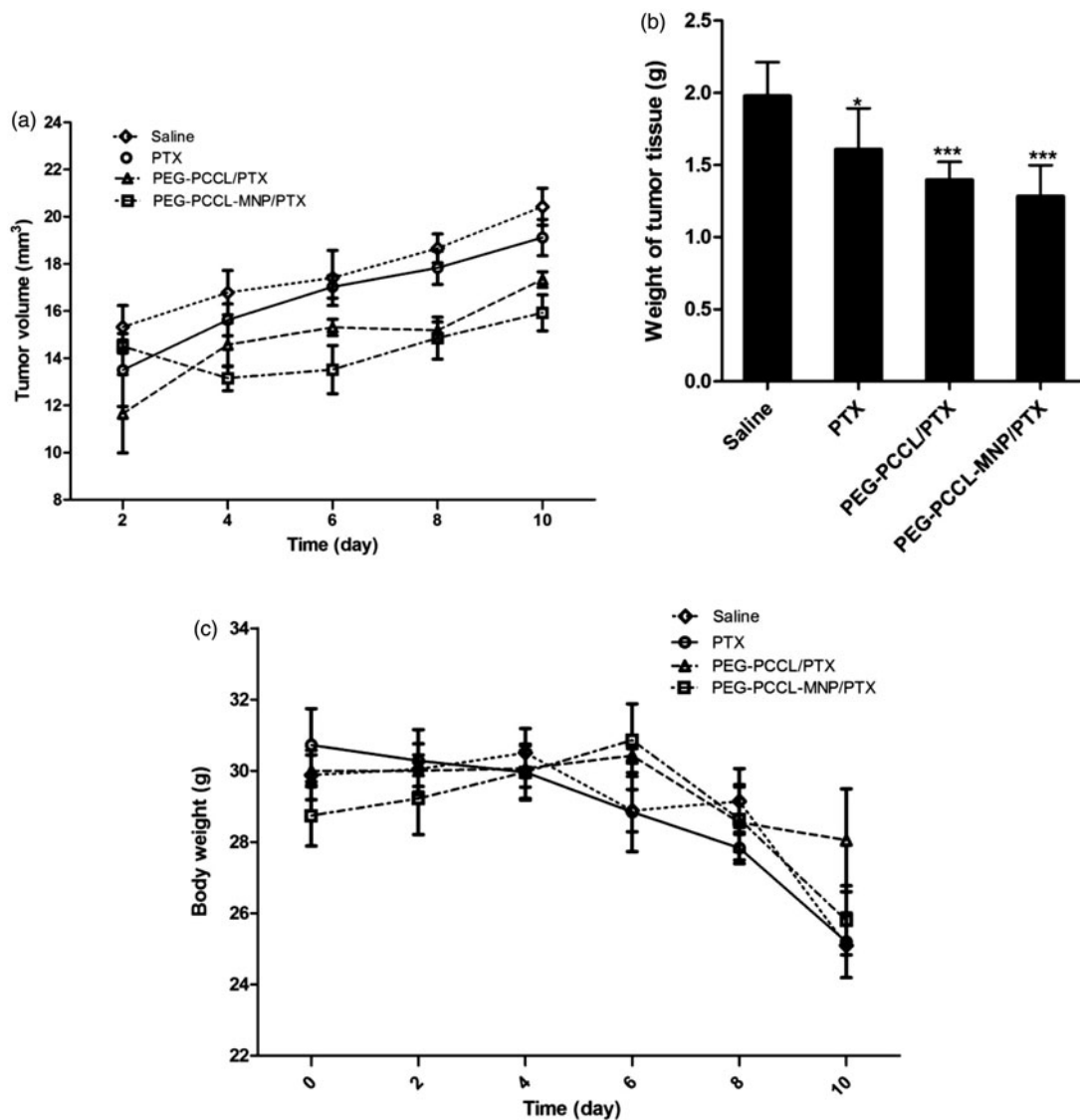


Figure 5. (A) The tumor growing curves for different treatment groups ($n = 5$). (B) The tumor weight of mice after treatments with different formulations ($n = 5$). Significant differences: * $p < .05$, *** $p < .001$, compared with the saline group. (C) The body weight of mice after treatments with different formulations ($n = 5$).

nuclei of the two cell lines were lateral located and complete and there was no observation of damage on the mitochondria, Golgi complex, and endoplasmic reticulum, thus showing little cytotoxicity and good biocompatibility of PEG-PCCL-MNP at the cellular level. In MTT assays (Figure 3(A,B)), there were no significant differences in the cell viability of HEK293 between PEG-PCCL and PEG-PCCL-MNP in all the test concentrations. However, when it comes to HepG2 liver tumor cells, PEG-PCCL-MNP showed less inhibition at the concentration of 0.25 and 0.5 mg/ml ($p < .05$) compared with PEG-PCCL, and at the concentration of 1.0 mg/ml PEG-PCCL-MNP showed more inhibition. Overall, the above results indicated that compared with PEG-PCCL, PEG-PCCL-MNP did not perform significant higher cytotoxicity on embryonic cells and showed more inhibition on the tumor cells at the comparatively high concentration. More importantly, PEG-PCCL-MNP effected the viability of HepG2 more than that of HEK293, which might be due to the tumor cells had higher metabolic activity leading to more cellular uptake than normal cells (Bossy-Wetzel &

Green, 2000) and this is the basis of entering into the clinical application. Hemolysis assays suggested that PEG-PCCL-MNP induced much less hemolysis of RBC than PEG-PCCL and normal saline, which might decrease their potential elimination by macrophages through phosphatidylserine- and scavenger receptor-mediated phagocytosis (Dobrovolskaia et al., 2008) and hence prolong their circulating time to enhance drug effect.

As for *in vivo* cytotoxicity assessments, rabbit phlebitis studies indicated that PEG-PCCL-MNP was non-toxicity and might be a candidate for its potential as an intravenous injected drug carrier in medicine fields. What's more, the H&E staining showed that compared with physiologic saline, PEG-PCCL and PEG-PCCL-MNP polymers did not induce obvious morphology change, acute tissue injury or inflammation reactions after 48 h treatment, indicating a relatively favorable histocompatibility. Interestingly, there should have been more nanoparticles due to the particle size and reticuloendothelial system scavenging in spleen, but there was no observation of obvious increase in amount or acute inflammation

reaction or lymphoid cell aggregation. We supposed that it was the permanent magnet which provided the external static magnetic field that decreased the distribution of the magnetic nanoparticle in the spleen. Besides, PEG-PCCL-MNP still maintained a relative high concentration in liver after 48 h while decreased in distribution in spleen when Prussian blue staining (Figure 4(c)), which is partly because liver are an organ with reticuloendothelial system cells (Bossy-Wetzel & Green, 2000) and the presence of external magnetic field lead higher superparamagnetic nanoparticle distributions in liver.

Furthermore, *in vivo* antitumor efficacy study showed that the tumor volume in the PEG-PCCL-MNP/PTX group was remarkably smaller than those of other groups, which indicated excellent tumor-specific cell targeting for drug delivery. From another point of view, body weight in the PTX and normal saline groups decreased rapidly (Figure 5(C)), which meant that *in vivo* toxicity of PEG-PCCL/PTX or PEG-PCCL-MNP/PTX was much lower than that of PTX. More interestingly, as Figure 4(d), not only massive apoptosis but also some bubbles-like structures could be observed in tumors tissues from the PEG-PCCL-MNP/PTX group, which indicated that the superparamagnetic nanoparticles group induced higher inhibition and injury on liver tumors. It was supposed that the increase in apoptosis in tumors treated with PEG-PCCL-MNP/PTX is a result of higher target with the presence of an external static magnetic field, which enhanced the effect of PTX instead of the toxicity of nanoparticle itself.

To sum up all experiments, on the one hand, owing to coated with PEG-PCCL, PEG-PCCL-MNP showed little *in vitro* or *in vivo* cytotoxicity and good biocompatibility. Especially when compared with our previous outcome PEG-PCCL, it did not decrease in histocompatibility, which was valuable to magnetic nanoparticles that is always harmful to organism. It also induced higher toxicity on tumor cells than normal cells, much less hemolysis and phlebitis, which all indicated that it might be a promising drug carrier candidate in clinical application. Moreover, physical modification rather than chemical modification was used in the procedure of coating, thus leading to less chemical residue through intravascular injection that may cause side effect. On the other hand, as the biodistribution behavior of intravenously injected magnetic nanoparticle drug carriers are greatly influenced by external magnetic field, higher biodistribution of PEG-PCCL-MNP in liver tissues indicated its effective tumor-specific cell targeting for drug delivery with the presence of external magnetic field, which in turn increase in apoptosis in tumors treated with it and loaded drugs. So with little cytotoxicity and excellent targeting, PEG-PCCL-MNP is a potential candidate of biocompatible and tumor-specific targeting drug vehicle for hydrophobic drugs. Definitely, dosing interval cannot be ignored which is closely related to controlled release. In this study, it was observed that the time of maximum concentration (T_{max}) was about 4 h. Additionally, the drug entrapment efficiency of PEG-PCCL-MNP was not satisfactory. So more research will be done to modify the nanoparticle to improve the EE and realize the controlled release of the drug, and further assays will be designed to test safety of the PEG-PCCL-MNP.

Disclosure statement

The authors report no conflicts of interest. The authors alone are responsible for the content and writing of this article.

Funding

This study is financially supported by the National Science Foundation Grant of China [No. J1103604].

References

- Bossy-Wetzel E, Green DR. (2000). Detection of apoptosis by annexin V labeling. *Meth Enzymol* 322:15–8.
- Cole AJ, David AE, Wang J, et al. (2011). Magnetic brain tumor targeting and biodistribution of longcirculating PEG-modified, cross-linked starch coated iron oxide nanoparticles. *Biomaterials* 32:6291–301.
- Cole AJ, Yang VC, David AE. (2011). Cancer theranostics: the rise of targeted magnetic nanoparticles. *Trends Biotechnol* 29:323–32.
- Danhier F, Lecouturier N, Vroman B, et al. (2009). Paclitaxel-loaded PEGylated PLGA-based nanoparticles: *in vitro* and *in vivo* evaluation. *J Control Release* 133:11–7.
- Del Vecchio S, Zannetti A, Fonti R, et al. (2007). Nuclear imaging in cancer theranostics. *Q J Nucl Med Mol Imaging* 51:152–63.
- Dobrovolskaia MA, Aggarwal P, Hall JB, McNeil SE. (2008). Preclinical studies to understand nanoparticle interaction with the immune system and its potential effects on nanoparticle biodistribution. *Mol Pharm* 5:487–95.
- Dobrovolskaia MA, Clogston JD, Neun BW, et al. (2008). Method for analysis of nanoparticle hemolytic properties *in vitro*. *Nano Lett* 8:2180–7.
- Elsaesser A, Howard CV. (2012). Toxicology of nanoparticles. *Adv Drug Deliv Rev* 64:129–37.
- Gou M, Men K, Shi H, et al. (2011). Curcumin-loaded biodegradable polymeric micelles for colon cancer therapy *in vitro* and *in vivo*. *Nanoscale* 3:1558–67.
- Gregory CD, Pound JD. (2010). Microenvironmental influences of apoptosis *in vivo* and *in vitro*. *Apoptosis* 15:1029–49.
- Kuang Y, Yuan T, Zhang Z, et al. (2012). Application of Ferriferous oxide modified by chitosan in gene delivery. *J Drug Deliv* 2012:920764.
- Larsen EK, Nielsen T, Wittenborn T, et al. (2009). Size-dependent accumulation of PEGylated silane-coated magnetic iron oxide nanoparticles in murine tumor. *ACS Nano* 3:1947–51.
- Li C, Cui J, Wang C, et al. (2008). Encapsulation of mitoxantrone into pegylated SUVs enhances its antineoplastic efficacy. *Eur J Pharm Biopharm* 70:657–65.
- Liu Y, Deng H, Xiao C, et al. (2014). Cytotoxicity of calcium rectorite micro/nanoparticles before and after organic modification. *Chem Res Toxicol* 27:1401–10.
- Liu Y, Samsonova O, Sproat B, et al. (2011). Biophysical characterization of hyper-branched polyethyleneimine-graft polycaprolactone-block-monomethoxy-poly (ethylene glycol) copolymers (hy-PEI-PCL-mPEG) for siRNA delivery. *J Control Release* 153:262–8.
- Luo Z, Jin L, Xu L, et al. (2016). Thermosensitive PEG-PCL-PEG (PECE) hydrogel as an *in situ* gelling system for ocular drug delivery of diclofenac sodium. *Drug Deliv* 23:63–8.
- Moore A, Marecos E, Bogdanov A Jr, Weissleder R. (2000). Tumoral distribution of long-circulating dextran-coated iron oxide nanoparticles in a rodent model. *Radiology* 214:568–74.
- Qiu JF, Gao X, Wang BL, et al. (2013). Preparation and characterization of monomethoxy poly(ethylene glycol)-poly(ϵ -caprolactone) micelles for the solubilization and *in vivo* delivery of luteolin. *Int J Nanomed* 8:3061–9.
- Rahman HS, Rasedee A, How CW, et al. (2013). Zerumbone-loaded nanostructured lipid carriers: preparation, characterization, and antileukemic effect. *Int J Nanomed* 8:2769–81.
- Rogošić M, Mencer HJ, Gomzi Z. (1996). Polydispersity index and molecular weight distributions of polymers. *Eur Polym J* 32:1337–44.
- Sun C, Du K, Fang C, et al. (2010). PEG-mediated synthesis of highly dispersive multifunctional superparamagnetic nanoparticles: their physicochemical properties and function *in vivo*. *ACS Nano* 4:2402–10.

- van Heerde WL, de Groot PG, Reutelingsperger CP. (1995). The complexity of the phospholipid binding protein Annexin V. *Thromb Haemost* 73:172–9.
- Wang J, Jia J, Liu J, et al. (2013). Tumor targeting effects of a novel modified paclitaxel-loaded discoidal mimic high density lipoproteins. *Drug Deliv* 20:356–63.
- Wang Z, Li M, Yu B, et al. (2012). Nanocalcium-deficient hydroxyapatite–poly (ϵ -caprolactone)–polyethylene glycol–poly (ϵ -caprolactone) composite scaffolds. *Int J Nanomed* 7:3123–31.
- Xie J, Lee S, Chen X. (2010). Nanoparticle-based theranostic agents. *Adv Drug Deliv Rev* 62:1064–79.
- Xu Y, Jin X, Ping Q, et al. (2010). A novel lipoprotein-mimic nanocarrier composed of the modified protein and lipid for tumor cell targeting delivery. *J Control Release* 146:299–308.
- Zhang W, Li C, Shen C, et al. (2016). Prodrug-based nano-drug delivery system for co-encapsulate paclitaxel and carboplatin for lung cancer treatment. *Drug Deliv* 23:2575–80.